

Upconversion in molecular hetero-nonanuclear lanthanide clusters in solution

Supplementary Information

Contents

S1. Synthesis and Characterisation	1
1.1 General Considerations	1
1.2. Experimental procedures and synthesis	3
<i>General procedure for the synthesis of $[Ln_9L_{16}(OX)_{10}](OX)$ ($X = H$ or D) clusters</i>	3
1.2.1 <i>Synthesis of $[Y_9L_{16}(OH)_{10}](OH)$</i>	3
1.2.2 <i>Synthesis of $[Yb_8TbL_{16}(OH)_{10}](OH)$ (H:H)</i>	4
1.2.3 <i>Synthesis of $[Yb_8TbL_{16}(OD)_{10}](OD)$ (D:D)</i>	4
S2. Supplementary Figures	5
<i>Figure S1. Top) Enlargement of the ES/MS spectrum displaying the region of the doubly charged polyhydrated clusters having lost one YL_1 unit ($[Y_8L_{15}(OH)_7(H_2O)_x]^{2+}$ (orange) or YL_2 unit ($[Y_8L_{14}(OH)_8(H_2O)_x]^{2+}$, with $x = 4$ to 7 (blue). Bottom) Enlargement of the ES/MS spectrum displaying the region of the triply charged polyhydrated clusters having lost one YL_3 unit ($[Y_8L_{13}(OH)_8(H_2O)_y]^{3+}$, with $y = 0$ to 7.....</i>	5
<i>Figure S2. 1H-NMR spectrum of the $[Y_9L_{16}(OH)_{10}](OH)$ complex. ($CDCl_3$, 600 MHz, 298K, see main text for the definition of endo and exo ligands).....</i>	6
<i>Figure S3. ^{13}C-NMR spectra of the $[Y_9L_{16}(OH)_{10}](OH)$ complex (126 MHz, 298K, $CDCl_3$).</i>	7
<i>Figure S4. HSQC NMR spectra of the $[Y_9L_{16}(OH)_{10}](OH)$ complex (500 MHz, 298K, $CDCl_3$).</i>	7
<i>Figure S5. HMQC NMR spectra of the $[Y_9L_{16}(OH)_{10}](OH)$ complex (500 MHz, 298K, $CDCl_3$).</i>	8
<i>Figure S6. ROESY NMR spectra of the $[Y_9L_{16}(OH)_{10}](OH)$ complex (600 MHz, 298K, $CDCl_3$).</i>	8
<i>Figure S7. DOSY NMR spectra of the $[Y_9L_{16}(OH)_{10}](OH)$ complex (600 MHz, 298K, $CDCl_3$).....</i>	9
<i>Figure S8. Top) Infrared absorption spectrum of $[Yb_8TbL_{16}(OH)_{10}](OH)$ (H:H), bottom) Infrared absorption spectrum of $[Yb_8TbL_{16}(OD)_{10}](OD)$ (D:D)</i>	10
<i>Figure S10. Powder XRD pattern of the isolated $[Tb_9L_{16}(OH)_{10}](OH)$ and $[TbYb_8L_{16}(OH)_{10}](OH)$ crystals.....</i>	11
<i>Figure S11. UV-Vis spectra of the mixed complexes</i>	11
<i>Figure S12. UC emission of the Yb_8Tb cluster (D:D) with a concentration of 1.5×10^{-6} M in CD_3OD ($\lambda_{exc} = 980$ nm, $P = 2.86$ W/cm2). Inset: UC emission with a concentration of 1×10^{-8} M ($\lambda_{exc} = 980$ nm, $P = 10.8$ W/cm2).</i>	12
S3. Details for the calculation of τ_{rad}	12
S4. DOSY NMR studies of $[Y_9L_{16}(OH)_{10}](OH)$	13
4.1 <i>DOSY calibration fit</i>	13
4.1.1 <i>Global calibration fit</i>	13
4.1.2 <i>Calibration fit of μ_3-OH</i>	13
4.1.3 <i>Calibration fit of H^b</i>	14
4.1.4 <i>Calibration fit of H^6</i>	14
4.1.5 <i>Calibration fit of H^a</i>	14
4.1.6 <i>Calibration fit of H^α</i>	15
S5. References	15

S1. Synthesis and Characterisation

1.1 General Considerations

Commercial grade chemicals and solvents were used without further purification unless otherwise stated. $CDCl_3$ was stored over activated 3 Å molecular sieves. The deuterated lanthanide salts for cluster syntheses ($LnCl_3 \cdot 6D_2O$), were obtained from the corresponding protic salt (0.89 mmol of $YbCl_3 \cdot 6H_2O$ and 0.11 mmol of $TbCl_3 \cdot 6H_2O$) dissolved in D_2O and evaporated (2 × 2 mL). Molecular sieves were activated by heating at 200 °C under dynamic vacuum for 18 hours. De-ionised water dispensed from a Millipore Milli-Q purification system was used in all cases. NMR spectra were

recorded with Bruker Avance 400 (400 MHz), Bruker Avance II 500 (500 MHz), or Bruker Avance III 600 (600 MHz) spectrometers. All chemical shift (δ) values are given in parts per million. ^1H and ^{13}C spectra are referenced to the solvent. All coupling constants are quoted in Hz. All ^{13}C spectra are proton decoupled unless otherwise stated. In cases where solvent mixtures are used, the main solvent is used as the reference. Infrared analyses were performed in the solid-state on an Agilent Cary 630 FTIR spectrophotometer. ESI-MS analyses were performed by Dr Jean-Marc Strub at the University of Strasbourg on a hybrid electrospray quadrupole time-of-flight mass spectrometer MS (Synapt G2 HDMS, Waters, Manchester, U.K.) coupled to an automated chip-based nanoelectrospray device (Triversa Nanomate, Advion Biosciences, Ithaca, U.S.A.) operating in the positive ion mode. The MS analysis was performed on the Synapt G2 HDMS instrument with external calibration using the singly charged ions produced by an ES-TOF tuning mix (G1969-85000, Agilent, U.S.A.). The nanoelectrospray device (Triversa Nanomate) was set at 1.5 kV on capillary and the pressure of the nebulizer gas was 0.55 psi. Elemental analyses were carried out by the Service Commun d'Analyses of the University of Strasbourg. ICP-AES analyses were performed using a Varian 720 ES instrument proceeded digestion in acid and are quoted as weight percentages. For the mixed hydrogen/deuterium clusters the experimental elemental compositions were compared to the calculated elemental compositions for both hydrogen and deuterium clusters. Spectroscopic measurements were performed with $10\times 10\text{ mm}^2$ quartz suprasil certified cells (Helma Analytics). UV/Vis absorption spectra were recorded on a Specord 205 (Analytic Jena) spectrometer and a lambda 950 UV/VIS/NIR absorption spectrometer from Perkin Elmer. Molar absorption coefficients are given as the average of at least two independent measurements. Steady-state emission spectra were recorded on an Edinburgh Instruments FLP920 working with a continuous 450 W Xe lamp and a red sensitive R928 photomultiplier from Hamamatsu in Pelletier housing for visible detection (230 to 900 nm) or a Hamamatsu R5 509-72 photomultiplier cooled at 77K for the Vis-NIR part. A 330 nm high pass cut-off filter was used to eliminate the second order artefacts for the visible part and an 850 nm high pass cut-off filter for the NIR part. Phosphorescence lifetimes were measured on the same instrument working in the Multi Channels Spectroscopy mode and using a Xenon flash lamp as the excitation source. Errors on the luminescence are estimated to $\pm 10\%$. Luminescence quantum yields were measured according to conventional procedures,¹ with diluted solutions (optical density < 0.05), using Rhodamine 6G in water ($\phi = 76.0\%$)² for Tb, Indocyanine green in MeOH ($\phi = 7.8\%$)³ for Yb and $[\text{Tb}(\text{Glu})\text{H}_2\text{O}]\text{Na}$ in water ($\phi = 31.0\%$)⁴ for the UC quantum yield as references.

Power dependent Tb UCL intensity was measured by integrating the Tb UCL intensity between 535 nm and 555 nm (1 nm increments, 2 s integration time, 5 nm slit bandpass) on a Fluorolog-3 fluorescence spectrometer (HORIBA scientific) using a MDL-III-980nm-2W laser (CNI Laser) with tuneable output power (2.1 W corresponds to 100%) and a beam size of ca. 5 mm x 8 mm as excitation source and a 5 mm path length quartz cuvette. First, the laser power was increased from 10 % to 100 % in steps of 10 % ("power up") and then the laser power was decreased from 95 % to 5 % in steps of 10 % ("power down"). Between each measurement the sample cuvette was removed from the spectrometer for at least 5 minutes to avoid sample heating at high excitation powers. The laser power was linear over the entire power range and for each 5 % step the laser power was measured using a laser power meter (Thorlabs).

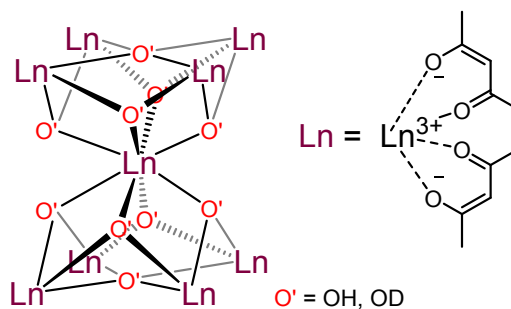
Tb UCL decay curves of Tb_1Yb_8 and Yb_9 at $542\pm 10\text{ nm}$ (bandpass filter 542/20 from Semrock) were measured in black multiwell plates (150 μL per well) on a time-resolved fluorescence plate reader (Edinburgh Instruments) using an MDL-

III-980nm-2W laser (CNI Laser) at *ca* 1.5 W and with a pulse width of 60 μ s. The PL intensities were collected in multichannel scaling mode in 0.5 μ s bins over 2 ms (4000 bins) and with a total acquisition time of 60 s at 200 Hz repetition rate.

Powder XRD was performed with a PANalytical Xpert Pro MRD diffractometer with Cu-K α 1 radiation ($\lambda = 1.540598$ Å) at 40 kV and 30 mA in θ/θ mode, reflection geometry. Energy-Dispersive X-ray Spectroscopy : The crystalline materials were observed by scanning electron microscopy with an FEI Quanta 250 FEG microscope in the microscopy centre CT μ of Lyon 1 University. The samples were mounted on stainless-steel pads and sputtered with carbon under high vacuum to prevent charging during the observations. Energy-dispersive X-ray spectroscopy was performed with an acceleration potential of 20 kV and 10 mm working distance.

1.2. Experimental procedures and synthesis

General procedure for the synthesis of $[\text{Ln}_9\text{L}_{16}(\text{OX})_{10}](\text{OX})$ (X = H or D) clusters



The compounds were synthesized according to a general procedure which has been modified from the literature.⁵

$\text{LnCl}_3 \cdot 6\text{X}_2\text{O}$ (Ln = Y³⁺ or Yb³⁺/Tb³⁺) (X = H, D; 1 mmol; 1.0 eq.) and acetylacetonate (205 μ L, 2.0 mmol, 2.0 eq.) was dissolved in CX_3OX (X = H or D; 5 mL). Et₃N (417 μ L, 3.0 mmol) was added dropwise and the reaction stirred at ambient temperature for one hour. The reaction was cooled to -18 °C and after several days a crystalline precipitate formed. The solid was filtered and washed with ice cooled CX_3OX (2 \times 2 mL) to give crystals suitable for analysis by single-crystal X-ray diffraction. The crystals were dried *in vacuo* to give of $[\text{Ln}_9\text{L}_{16}(\text{OX})_{10}](\text{OX})$ as white microcrystalline powders.

1.2.1 Synthesis of $[\text{Y}_9\text{L}_{16}(\text{OH})_{10}](\text{OH})$

Prepared by the general procedure using $\text{YCl}_3 \cdot 6\text{H}_2\text{O}$ (303 mg) and CH_3OH to give the title compound (123 mg, 48 μ mol, 43%). ¹H NMR (400 MHz, 298 K, CDCl_3): δ 6.74 (br. s, 8H, μ_3 -OH), 5.47 (s, 8H, C(O)CH^bC(O)), 5.22 (s, 8H, C(O)CH^βC(O)), 3.22 (br. s, 2H, μ_4 -OH), 1.74 (s, 48H, C(O)CH^α₃), 1.57 (s, 48H, C(O)CH^α₃). ¹³C NMR (126 MHz, 298 K, CDCl_3): δ 194.8 (br. s, C^c(O)), 190.7 (br. s, C^v(O)), 189.2 (br. s, C^v O), 186.2 (br. s, C^c(O)), 103.6 (br. s, C(O)C^bHC(O)), 101.1 (br. s, C(O)C^βHC(O)), 27.5 (s, C(O)C^αHC(O)), 26.5 (br. s, C(O)C^αH₃), 26.0 (br. s, C(O)C^αH₃). ESI-MS *m/z* calcd. for $[\text{C}_{80}\text{H}_{122}\text{O}_{42}\text{Y}_9]^+$ 2554.8938 found 2554.8901. Anal. Calcd for $[\text{Y}_9\text{L}_{16}(\text{OH})_{10}](\text{OH}) \cdot 4\text{H}_2\text{O}$: C₈₀H₁₃₁O₄₇Y₉ (2645.04 g mol⁻¹): C, 36.33; H, 4.99; N, 0.00. Found: C, 35.98; H, 4.84; N, 0.00. IR (ATR): ν_{max} 3303 (OH), 2291 (CH), 2254 (CH), 2916 (CH), 1616 (C=O), 1586 (C=O), 1506, 1379, 1357, 1253, 1189, 1014, 922 cm⁻¹.

1.2.2 Synthesis of $[\text{Yb}_8\text{TbL}_{16}(\text{OH})_{10}](\text{OH})$ (H:H)

Prepared by the general procedure using $\text{YbCl}_3 \cdot 6\text{H}_2\text{O}$ (344 mg, 0.89 mmol) and $\text{TbCl}_3 \cdot 6\text{H}_2\text{O}$ (41 mg, 0.11 mmol) and CH_3OH to give the title compound. Anal. Calcd for $[\text{Yb}_8\text{TbL}_{16}(\text{OH})_{10}](\text{OH}) \cdot 6\text{H}_2\text{O}$: $\text{C}_{80}\text{H}_{135}\text{O}_{49}\text{Tb}_1\text{Yb}_8$ (3424.26 g mol⁻¹): C, 28.06; H, 3.97; N, 0.00; Found: C, 28.08; H, 3.76; N, 0.00. IR (ATR): ν_{max} 3316 (OH), 2988 (CH), 2955 (CH), 2914 (CH), 1613 (C=O), 1585 (C=O), 1500, 1380, 1356, 1269, 1254, 1014, 923 cm⁻¹. ICP-AES: calcd. Tb, 4.64%; Yb, 40.4%; Found: Tb, 4.60 ± 0.06%; Yb, 40 ± 1%.

1.2.3 Synthesis of $[\text{Yb}_8\text{TbL}_{16}(\text{OD})_{10}]\text{OD}$ (D:D)

Prepared by the general procedure using $\text{YbCl}_3 \cdot 6\text{D}_2\text{O}$ (0.89 mmol) and $\text{TbCl}_3 \cdot 6\text{H}_2\text{O}$ (0.11 mmol) and CD_3OD to give the title compound. Anal. Calcd for $[\text{Yb}_8\text{TbL}_{16}(\text{OD})_{10}](\text{OD}) \cdot 4\text{H}_2\text{O}$: $\text{C}_{80}\text{H}_{120}\text{D}_{11}\text{O}_{47}\text{Yb}_8\text{Tb}$ (3399.30 g mol⁻¹): C, 28.27; H, 4.21; N, 0.00. Found: C, 27.97; H, 3.75; N, 0.00. IR (ATR): ν_{max} 3316 (OH), 3121 (OH), 2990 (CH), 2959 (CH), 2915 (CH), 2439 (OD), 1607 (C=O), 1580 (C=O), 1484, 1377, 1356, 1252, 1014, 918 cm⁻¹; ICP-AES: calcd. Tb, 4.7%; Yb, 41%; Found: Tb, 4.4 ± 0.2%; Yb, 39 ± 2%.

S2. Supplementary Figures

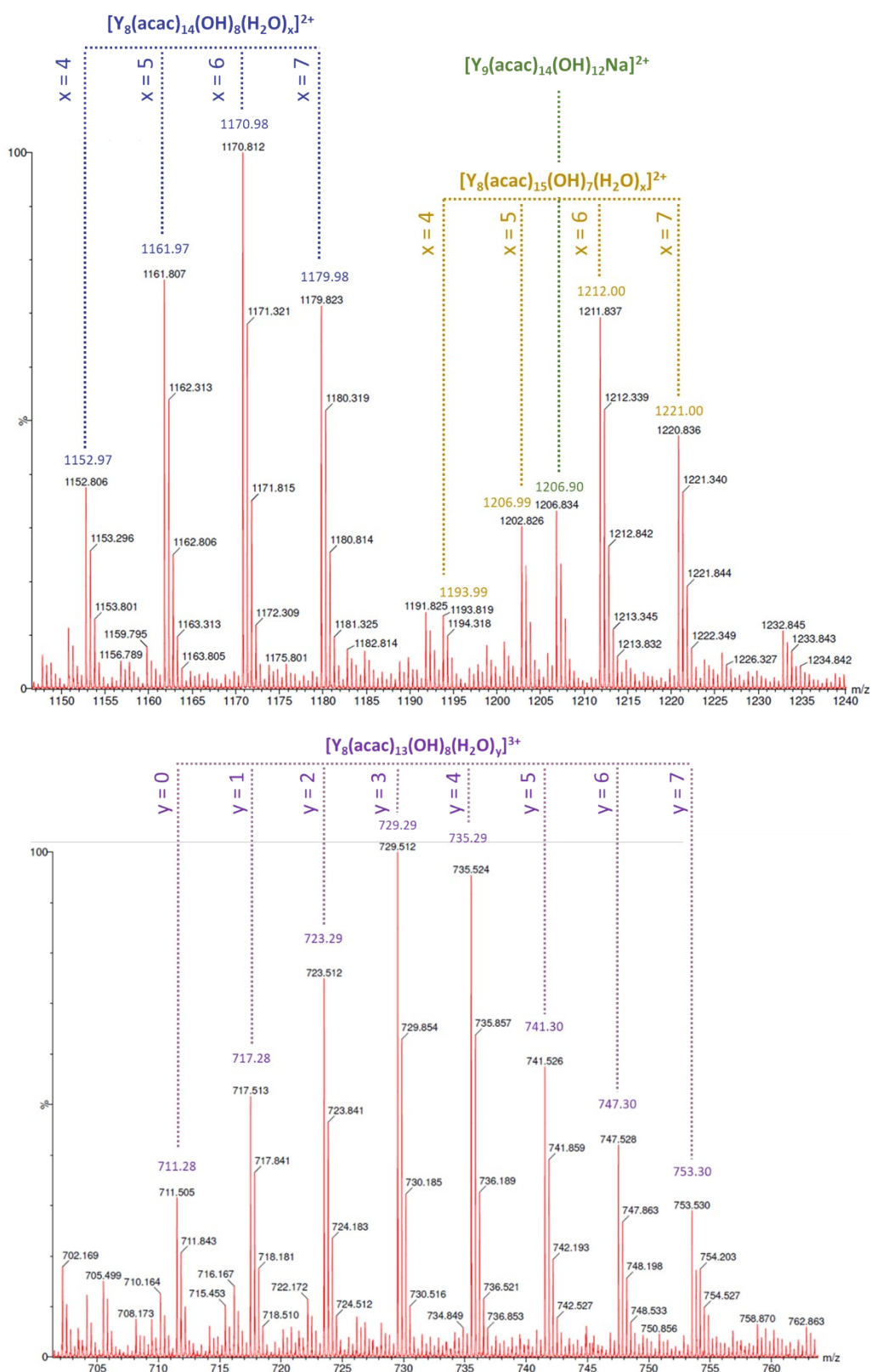


Figure S1. Top) Enlargement of the ES/MS spectrum displaying the region of the doubly charged polyhydrated clusters having lost one YL_1 unit ($[Y_8L_{15}(OH)_7(H_2O)_x]^{2+}$ (orange) or YL_2 unit ($[Y_8L_{14}(OH)_8(H_2O)_x]^{2+}$, with $x = 4$ to 7 (blue). Bottom) Enlargement of the ES/MS spectrum displaying the region of the triply charged polyhydrated clusters having lost one YL_3 unit ($[Y_8L_{13}(OH)_8(H_2O)_y]^{3+}$, with $y = 0$ to 7 .

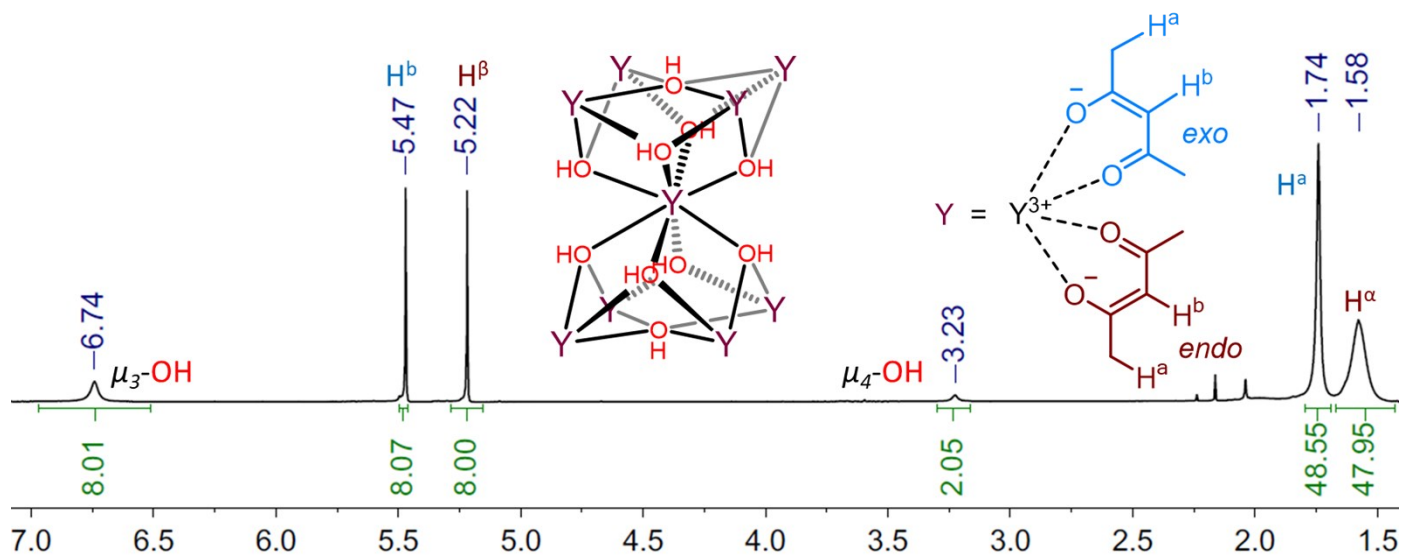


Figure S2. $^1\text{H-NMR}$ spectrum of the $[\text{Y}_9\text{L}_{16}(\text{OH})_{10}](\text{OH})$ complex. (CDCl_3 , 600 MHz, 298K, see main text for the definition of *endo* and *exo* ligands).

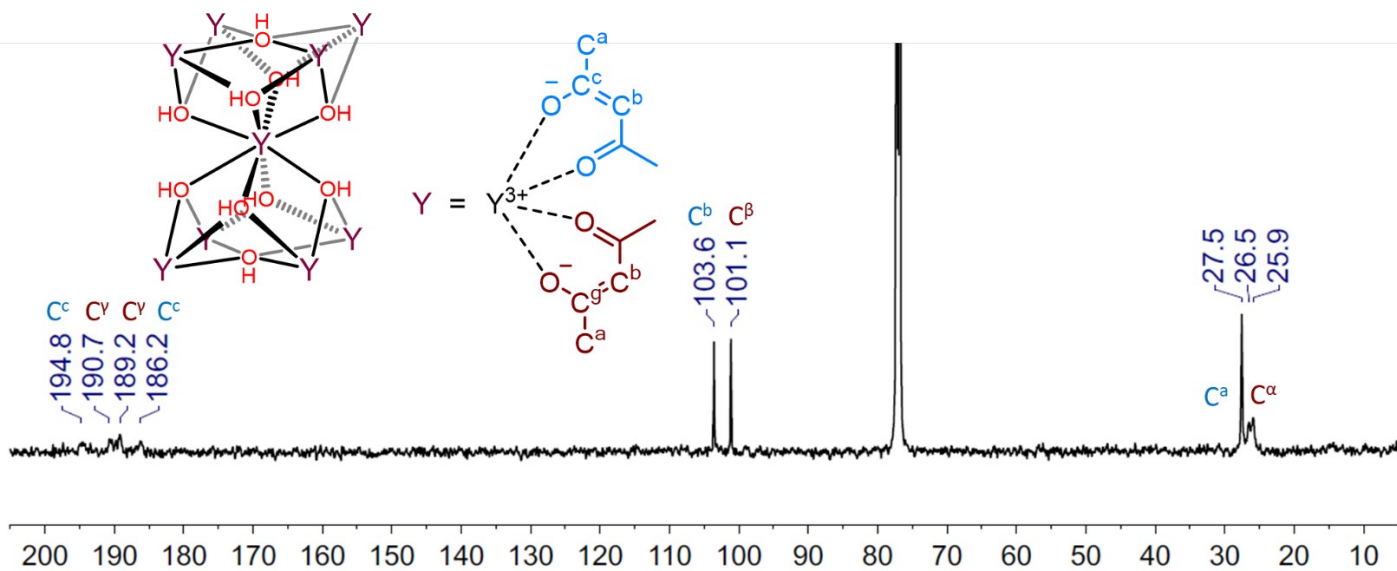


Figure S3. ^{13}C -NMR spectra of the $[\text{Y}_9\text{L}_{16}(\text{OH})_{10}](\text{OH})$ complex (126 MHz, 298K, CDCl_3).

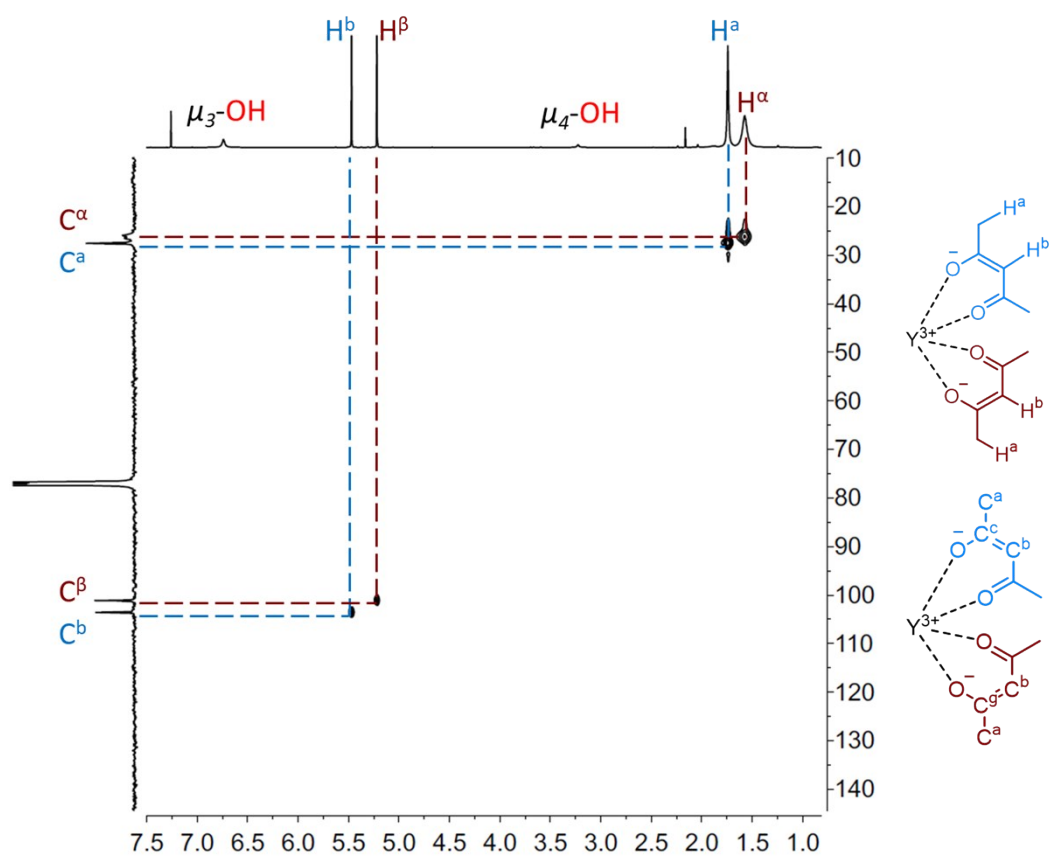


Figure S4. HSQC NMR spectra of the $[\text{Y}_9\text{L}_{16}(\text{OH})_{10}](\text{OH})$ complex (500 MHz, 298K, CDCl_3).

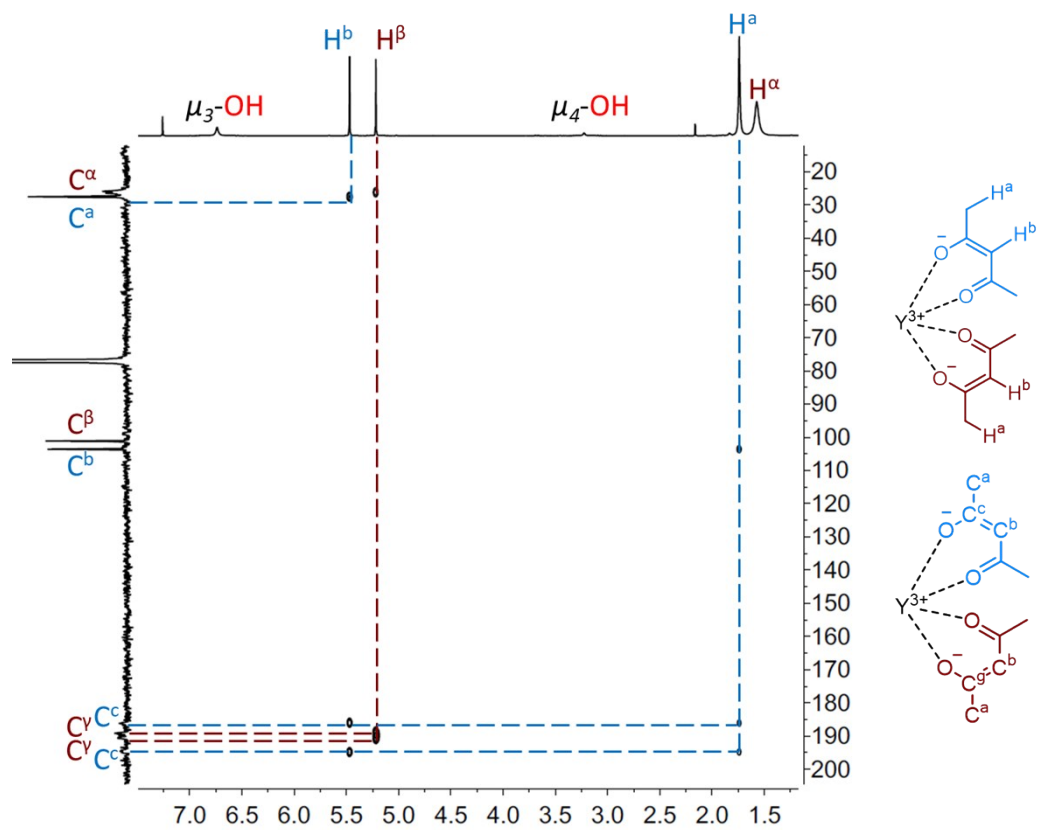


Figure S5. HMQC NMR spectra of the $[Y_9L_{16}(OH)_{10}](OH)$ complex (500 MHz, 298K, $CDCl_3$).

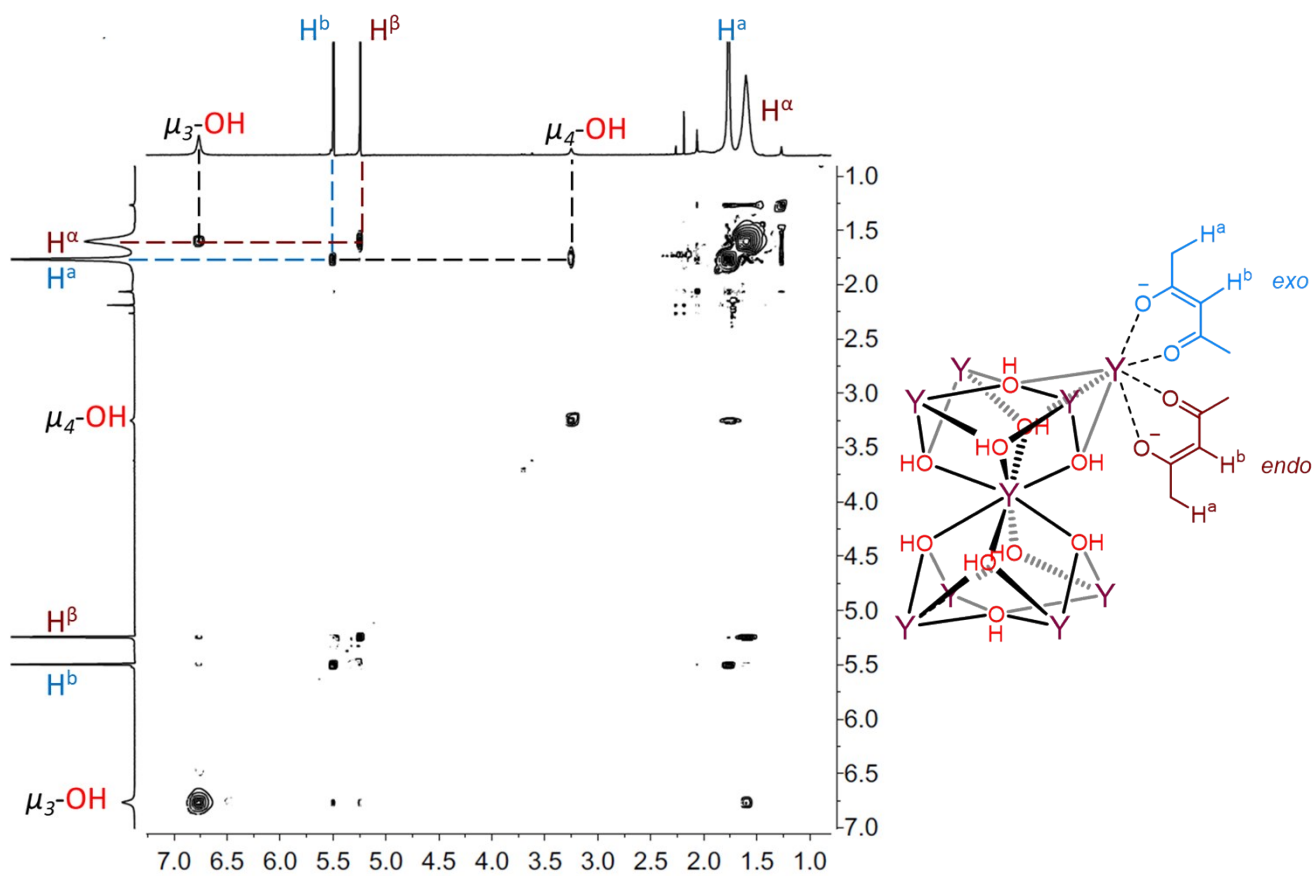


Figure S6. ROESY NMR spectra of the $[Y_9L_{16}(OH)_{10}](OH)$ complex (600 MHz, 298K, $CDCl_3$).

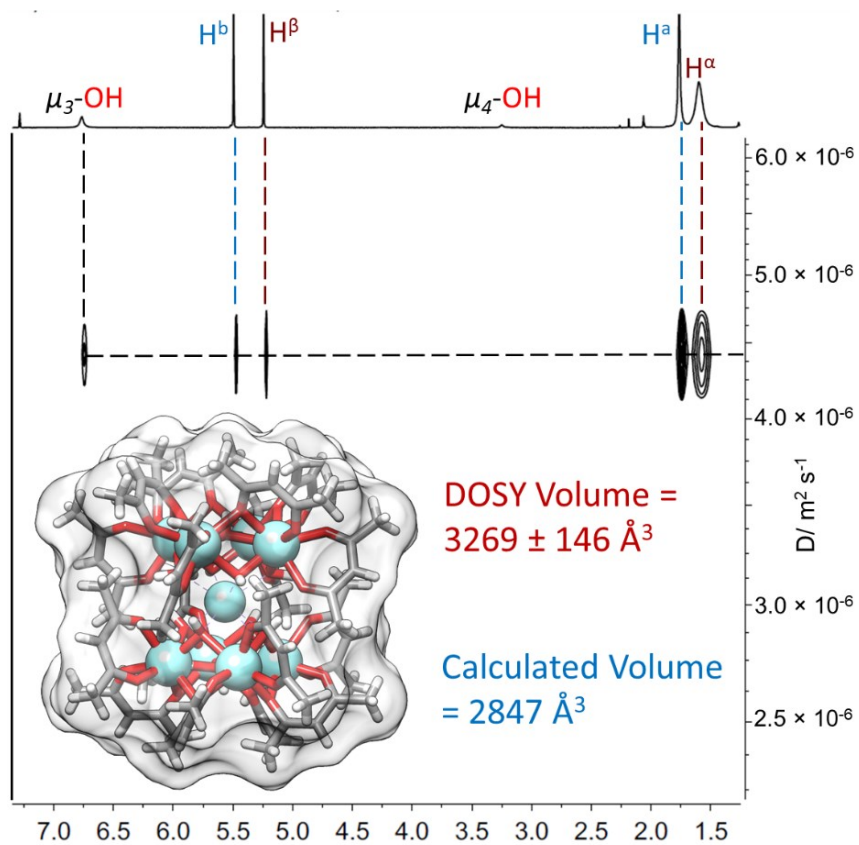
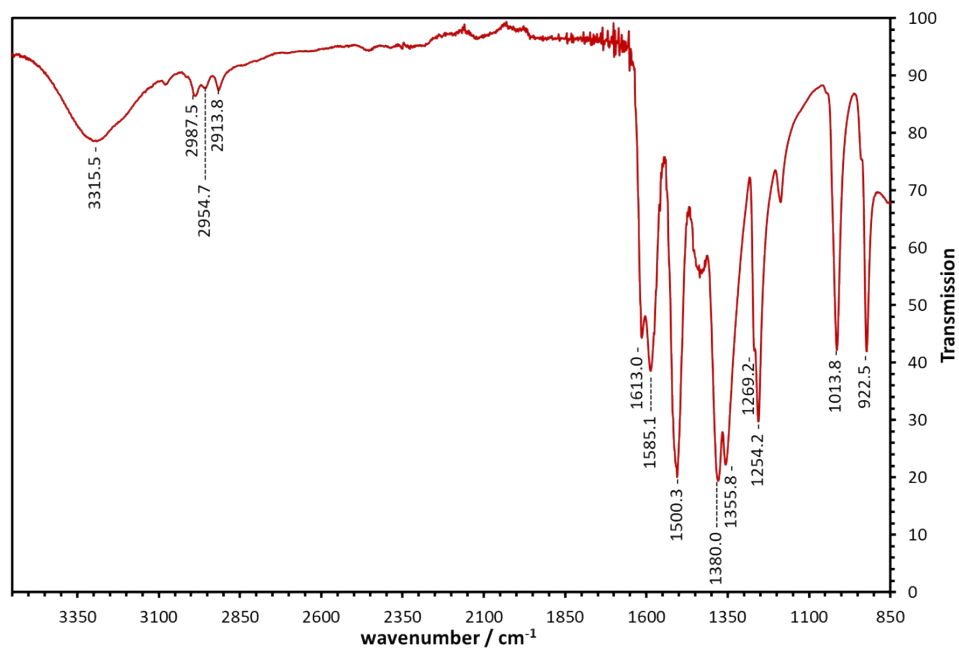


Figure S7. DOSY NMR spectra of the $[\text{Y}_9\text{L}_{16}(\text{OH})_{10}](\text{OH})$ complex (600 MHz, 298K, CDCl_3).



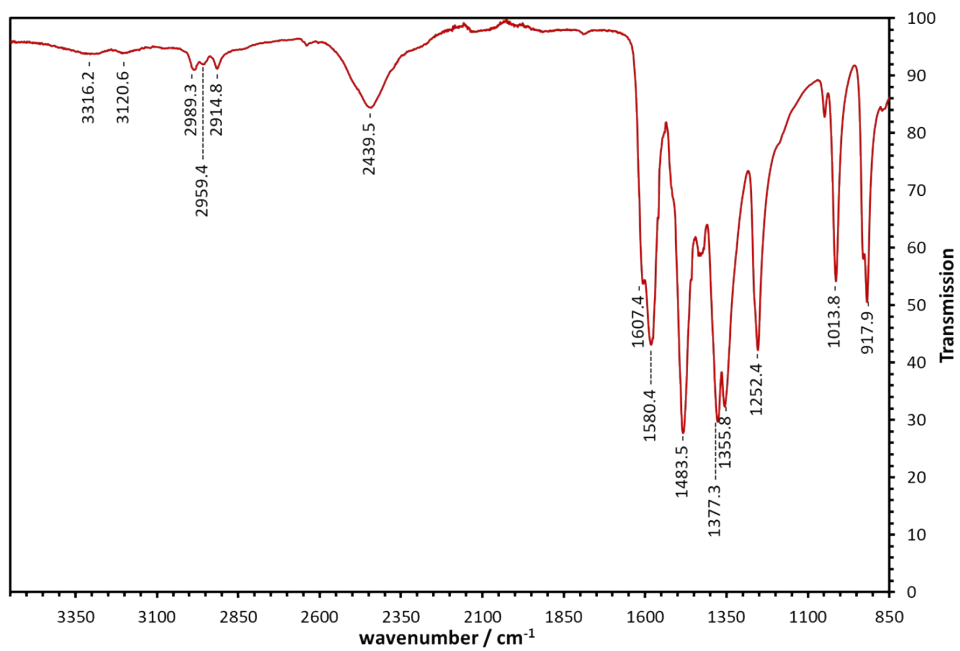


Figure S8. Top) Infrared absorption spectrum of $[\text{Yb}_8\text{TbL}_{16}(\text{OH})_{10}](\text{OH})$ (H:H), bottom) Infrared absorption spectrum of $[\text{Yb}_8\text{TbL}_{16}(\text{OD})_{10}](\text{OD})$ (D:D)

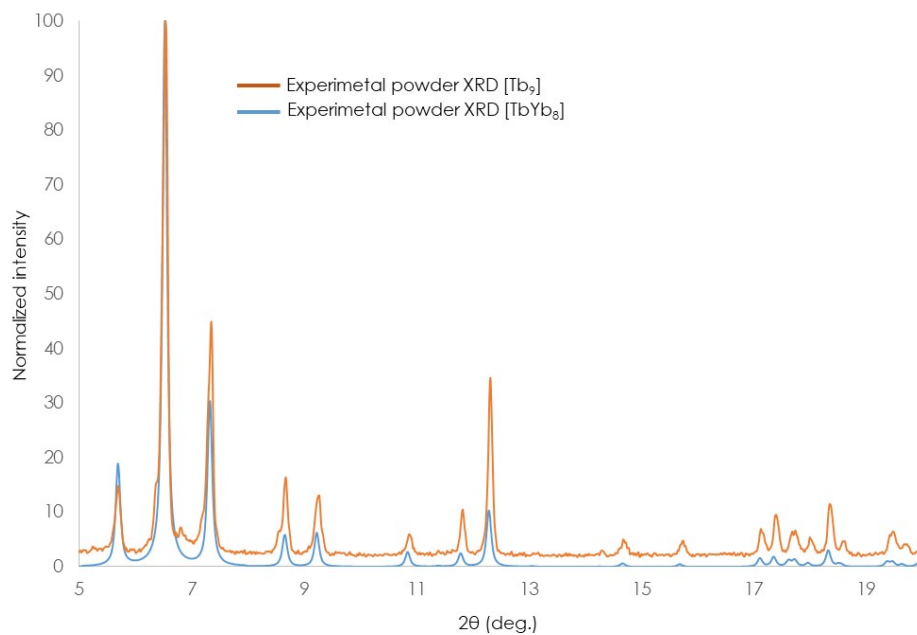


Figure S9. Powder XRD pattern of the isolated [Tb₉L₁₆(OH)₁₀](OH) and [TbYb₈L₁₆(OH)₁₀](OH) crystals.

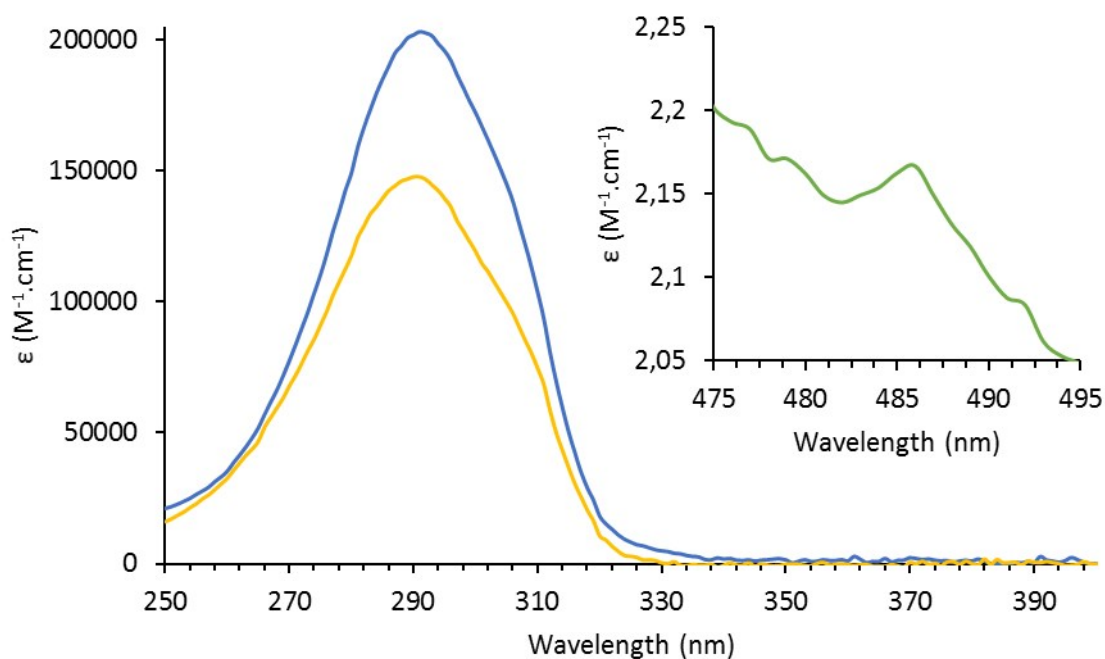


Figure S10. UV-Vis spectra of the mixed complexes D:D (blue); and H:H (yellow) (see main text for their classification) in MeOH; Inset: Enlargement of the visible part of the absorption spectra of the Tb ⁵D₄ → ⁷F₆ transition (C = 22.8 mM, D:D)

ϵ_{ij}^{band}		ϵ_{Yb}	$\tau_{Yb}/\mu s$	τ_{radYb}	$\tau_{Tb}/ms(\%)$	ϕ_{Yb}^c	ϕ_{Tb}^d	$\phi_{UC}^{a,e}$
$/\times 10^{-4} M^{-1} \cdot cm^{-1}$	$/M^{-1} \cdot cm^{-1}$	$/M^{-1} \cdot cm^{-1}$	b	$/\mu s$	b	$/\%$	$(\%)$	$(\times 10^7)$
(λ/nm)								
D:D	20.3 (291)	44.6	<1	632	0.926	0.091		
		48.5 ^a	16.6 ^a	683 ^a	0.35(5%)/1.12(95%) ^a	0.57 ^a	2.7	1
H:H	14.8 (291)	46.9	<1	578	0.947	0.080	1.5	0.056
		51.7 ^a	15.6 ^a	663 ^a	0.25(4%)/1.14(96%) ^a			

Table S1. Photophysical properties of the different clusters (MeOH, unless otherwise stated).

^a Values obtained in CD₃OD. ^b excitation at 340 nm (CD₃OD - concentrated solutions) and at 292 nm (MeOH - diluted solutions). ^c using cardiogreen (IR125) in MeOH ($\Phi = 0.078$) as reference.² ^d Using Rhodamine6G in water ($\Phi = 0.76$; $\lambda_{exc} = 488$ nm) as reference.³ ^e Excitation at 980 nm ($P = 2.86$ W/cm²), using [Tb(Glu)H₂O]Na in water ($\Phi=0.31$) as reference for the up-conversion quantum yield.⁴

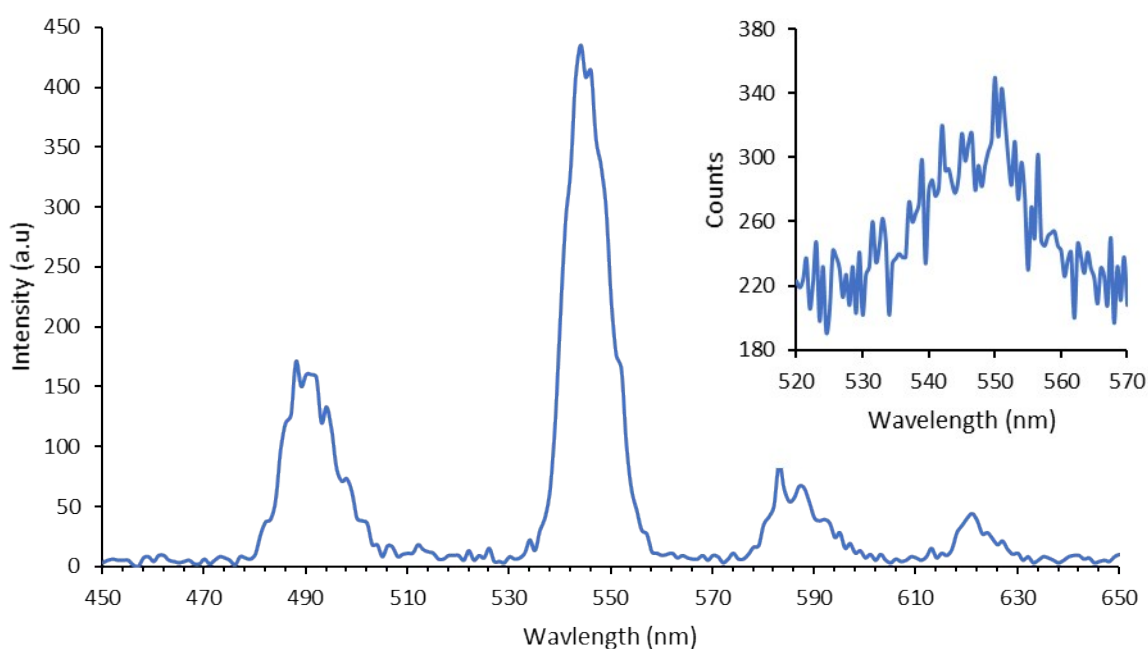


Figure S11. UC emission of the Yb₈Tb cluster (D:D) with a concentration of 1.5×10^{-6} M in CD₃OD ($\lambda_{exc} = 980$ nm, $P = 2.86$ W/cm²). Inset: UC emission with a concentration of 1×10^{-8} M ($\lambda_{exc} = 980$ nm, $P = 10.8$ W/cm²).

S3. Details for the calculation of τ_{rad} .

From the NIR absorption band of Yb and weighting the absorption coefficients by the number of Yb atoms, it was possible to calculate the radiative lifetime of Yb, τ_{rad} , using the equation:

$$\frac{1}{\tau_{rad}} = 2303 \times \frac{8\pi c n^2 \nu_{ul}^2}{N_A} \frac{g_l}{g_u} \int \epsilon(\nu) d\nu \quad \text{where} \quad \nu_{ul} = \frac{\int \nu \times \epsilon(\nu) d\nu}{\int \epsilon(\nu) d\nu}$$

c being the speed of light in a vacuum, n the refractive index of the medium, N_A Avogadro's number, ν_{ul} the barycenter of the transition (cm^{-1}), $g_i=2J_i + 1$ are related to the degeneracies of the upper (u , $J_u=5/2$) and lower (l , $J_l=7/2$) excited states of Yb, and $\epsilon(\nu)$ is the molar absorption coefficient at the wavenumber ν .

S4. DOSY NMR studies of $[\text{Y}_9\text{L}_{16}(\text{OH})_{10}](\text{OH})$

DOSY NMR studies were performed on a Bruker Avance III 600 MHz NMR spectrometer using a 15 mM solution of $[\text{Y}_9\text{L}_{16}(\mu_3\text{-OH})_8(\mu_4\text{-OH})_2](\text{OH})$ in CDCl_3 using a 3 mm NMR tube.

4.1 DOSY calibration fit

4.1.1 Global calibration fit

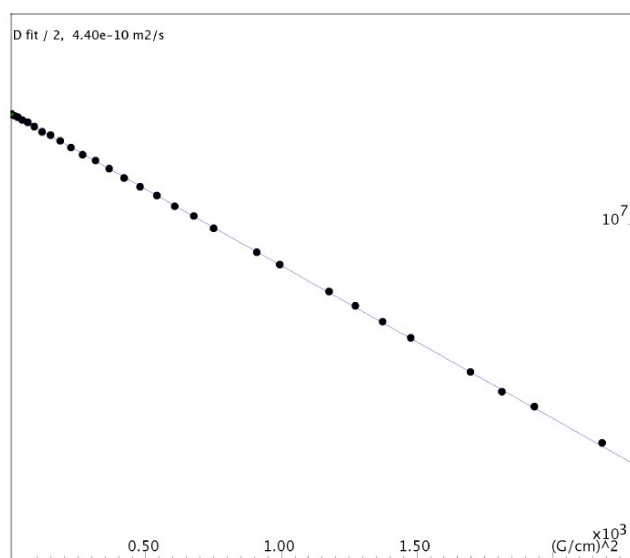


Figure S12. Global DOSY calibration fit

4.1.2 Calibration fit of $\mu_3\text{-OH}$

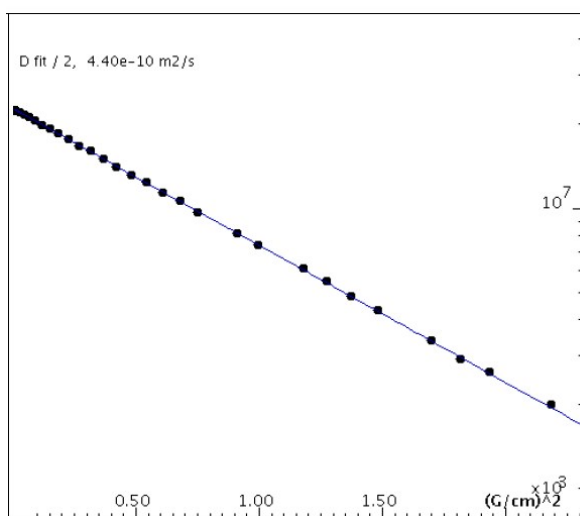


Figure S13. DOSY calibration fit for $\mu_3\text{-OH}$

4.1.3 Calibration fit of H^b

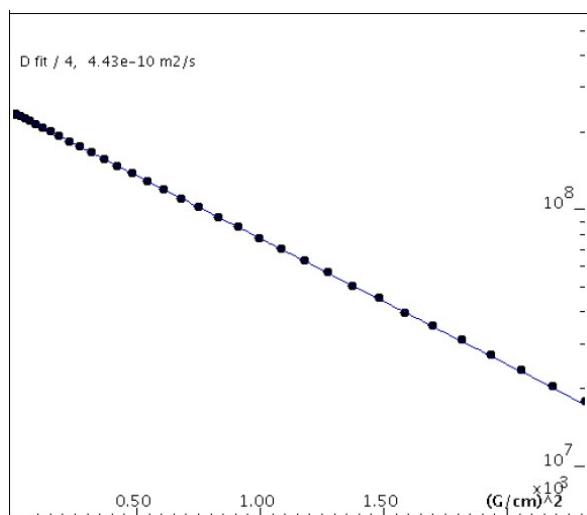


Figure S14. DOSY calibration fit for H^b

4.1.4 Calibration fit of H^b

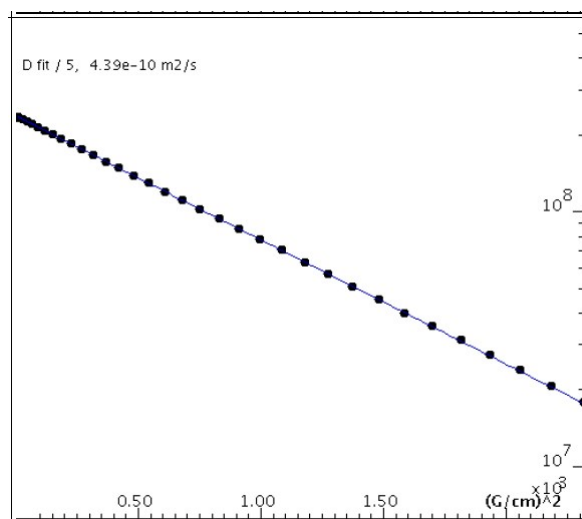


Figure S15. DOSY calibration fit for H^b

4.1.5 Calibration fit of H^a

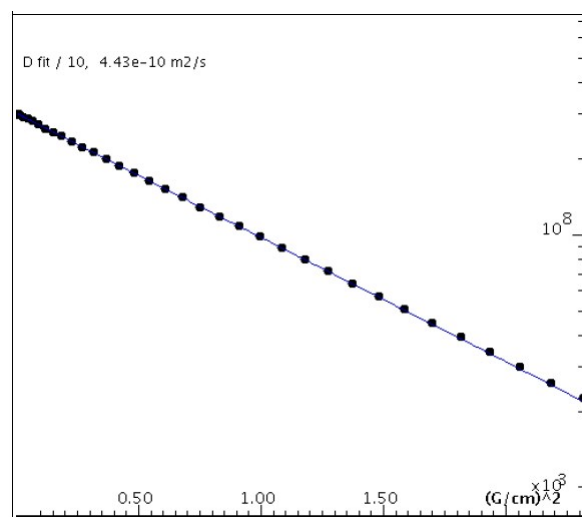


Figure S16. DOSY calibration fit for H^a

3.1.6 Calibration fit of H^α

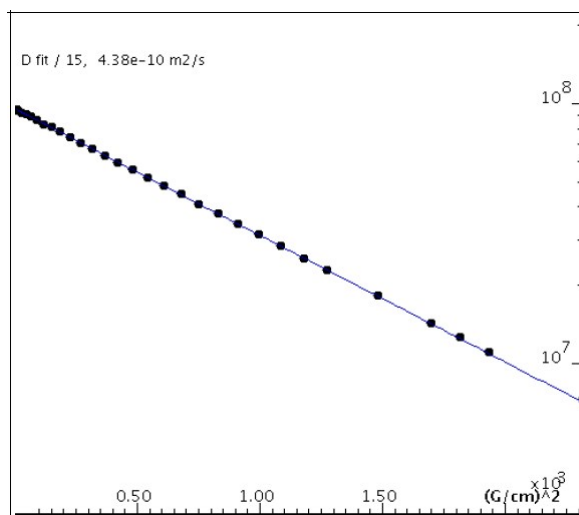


Figure S17. DOSY calibration fit for H^α

S5. References

-
- ¹ B. Valeur, M. N. Berberan-Santos. *Molecular Fluorescence: Principles and Applications*, 2nd ed., Wiley-VCH, Weinheim, **2013**.
 - ² J. Olmsted, *J. Phys. Chem.* **1979**, *83* (20), 2581–2584.
 - ³ R. C. Benson, H. A. Kues, *Phys. Med. Biol.* **1978**, *23* (1), 159–163.
 - ⁴ N. Weibel, L. C. Charbonnière, M. Guardigli, A. Roda, R. Ziessel, *J. Am. Chem. Soc.* **2004**, *126*, 4888–4896.
 - ⁵ S. Petit, F Baril-Robert, G. Pilet, C. Reber, D. Luneau, *J. Chem. Soc. Dalt. Trans.* **2009**, *34*, 6809–6815.
 - ⁶ M.H.V. Werts, R.T.F. Jukes, J.W. Verhoeven, *Phys. Chem. Chem. Phys.*, 2002, *4*, 1542–1548.